QUASINEUTRAL BEAM PROPAGATION IN SPACE

K. Papadopoulos,* A. Mankofsky and A. Drobot

Science Applications International Corporation, 1710 Goodridge Drive, McLean, Virginia 22102

Abstract. The propagation of dense energetic neutralized ion beams or plasmoids injected into a plasma across the ambient magnetic field under ionospheric conditions is considered. Using a simple physical model supported by two-dimensional hybrid simulations, it is shown that thin dense beams can propagate ballistically over lengths many times their gyroradius. This occurs when the following conditions are satisfied: $\Delta/R_o \ll 1$, where Δ is the cross field beam width and R_o the gyroradius of an ambient ion having a velocity equal to the beam velocity u_b, and $n_b M_b/n_o M_o \gg 1$, where $n_b(M_b)$, $n_o(M_o)$ are the density (mass) of beam and ambient ions. The scaling of the ballistic propagation lengths and times with beam and ambient parameters is presented along with comments on the applicability of the model to space and astrophysics.

Introduction

The propagation of high speed neutralized ion beams, often called plasmoids, across a magnetic field is among the oldest of problems in plasma physics. It first arose in investigations of the origin of magnetospheric storms and substorms [Chapman and Ferraro, 1931; Ferraro, 1952]. Despite the long history of investigation, a clear model has yet to emerge. Early theoretical models established by Chapman and Ferraro [1931], Ferraro [1952], Tuck [1959] and Chapman [1960], indicated that a neutralized beam with a large width Δ transverse to the ambient magnetic field $\mathbf{B}_o$($\Delta \gg R_b$, where R_b is the gyroradius of the beam ions), will in general compress the magnetic field but will not propagate significantly. Propagation can potentially occur in the diamagnetic regime when $\beta_b \equiv 4\pi n_b M_b u_b^2/B_o^2 \gg 1$, where n_b, M_b, u_b are the density, mass and cross field velocity of the beam ions. This propagation mode can be properly described by MHD and is equivalent to the propagation of a solid conductor moving across $\mathbf{B}_o$. During propagation the beam picks up and carries along the ambient plasma and magnetic field, in a fashion similar to the pick-up of cometary ions by the solar wind [Cargill et al., 1988]. The mass loading, along with the various pick-up ring instabilities, soon destroys the beam coherence. Another propagation mode proposed by Schmidt [1960] addressed the narrow beam regime, $R_e < \Delta \ll R_b$ where R_e is the electron gyroradius. This propagation mode occurs in the non-diamagnetic $\beta_b \ll 1$ regime (often called the electrostatic regime). In this case the flow energy is not sufficient to alter the magnetic field configuration; therefore, the ambient magnetic field controls the electron and ion dynamics. A polarization electric field develops by the differential motion of the magnetized electrons ($R_e \ll \Delta$) and the unmagnetized ions ($R_b > \Delta$). The polarization field $\mathbf{E}$, coupled with the ambient field $\mathbf{B}_o$, allows the neutralized beam to move by an $\mathbf{E} \times \mathbf{B}_o$ drift [Schmidt, 1960]. This mode of propagation was experimentally observed by Baker and Hammel [1965]. Peter and Rostoker [1982] noted that dielectric shielding due to the presence of an ambient plasma does not affect the beam propagation as long as $V_{Ap}/V_{Ab} < 1$, where V_{Ab}, V_{Ap} are the beam and plasma Alfvén speeds. Scholer's [1970] model of artificial propagation of ion clouds in the magnetosphere belongs to this class of low kinetic β, subalfvénic propagation modes.

In this paper we examine plasmoid propagation in the narrow beam regime discussed by Schmidt [1960] but for the high $\beta_b(\beta_b \gg 1)$ strongly diamagnetic case. It will be shown first by a simple analytic model, and then by a set of 2-D computer simulations using a hybrid code [Mankofsky et al., 1987], that extremely long range propagation across the magnetic field is possible in the strongly diamagnetic $\beta_b \gg 1$ regime if $n_b \gg n_o$ and $R_e \ll \Delta < u_b/\Omega_o \equiv R_o$, where Ω_o is the cyclotron frequency of the ambient plasma ions. The propagation physics and the

* Permanent Address: Department of Physics, University of Maryland, College Park, Maryland 20742.

self-similar stationary field configurations are completely different from the high β_b MHD regime. Preliminary results on this propagation mode appeared recently [Papadopoulos et al., 1988].

In the MHD regime where the beam width is much larger than the beam ion gyroradius, R_b, we expect the background field to be excluded by ion diamagnetic effects. As a consequence the background plasma and magnetic field will be swept by the beam resulting in strong coupling at the beam front. In the low β_b situation described by Schmidt where the beam propagates because of the presence of a polarization electric field the interpenetration of the beam by the background plasma is also likely to lead to strong coupling and hence poor propagation. However, for a high β ion beam which is narrower than its ion gyroradius, the possibility exists for diverting the background plasma and magnetic field asymmetrically around the beam with minimum coupling or beam-background interpenetration. In this situation the high β_b ions have sufficient energy to displace the background plasma at the beam head. Intuitively we expect the beam front to erode at a small rate while the beam body remains undisturbed.

Propagation Model - Physical Description

Consider a cold, dense ($n_b \gg n_o$), high kinetic beta ($\beta_b \gg 1$) ion beam interacting with an ambient magnetoplasma such as shown in Fig. 1. It is convenient to perform our analysis in the beam reference frame. In this frame for $\mathbf{B}_o = B_o\hat{e}_y$, the ambient magnetized plasma flows with a cross field velocity $\mathbf{u}_o = -u_b\hat{e}_z$, with the aid of a motional electric field $\mathbf{E} = -(\mathbf{u}_e \times \mathbf{B}_o)/c = -\hat{e}_x(u_b B_o)/c$, where $\mathbf{u}_e$ is the fluid velocity of the plasma electrons and of the magnetic flux. The equations of motion of the background plasma ions (charge e, mass M_o) are

$$\frac{du_x}{dt} = \frac{e}{M_o}\left[E_x - \frac{u_x B_y}{c}\right] , \tag{1a}$$

$$\frac{du_z}{dt} = \frac{e}{M_o}\left[E_z + \frac{u_x B_y}{c}\right] . \tag{1b}$$

The value of the motional electric field $E_x(z)$ is given by

$$\mathbf{E}(z) = -\frac{\mathbf{u}_e(z) \times \hat{e}_y B(z)}{c} = \hat{e}_x \frac{u_e(z)B(z)}{c} . \tag{2}$$

In the region $z > 0$ ahead of the beam-plasma interface (Fig. 1a), $u_e(z) = -u_b$ and $u_z = -u_b$ so that the r.h.s. of (1a) is zero. Namely, the ions, the electrons and the flux follow straight ballistic orbits. At the plasma interface,

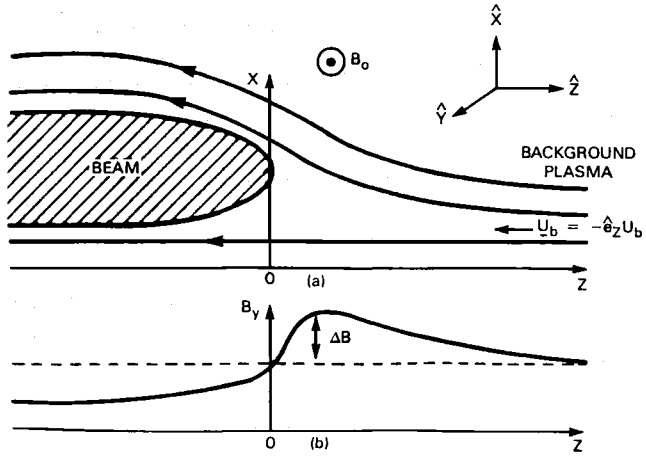

Fig. 1. A schematic of the physics involved during the interaction of the ion beam with the background plasma.

$z \approx 0$, the fluid velocity u_e reduces to

$$u_e(z) = \frac{n_o u_b}{n_o + n_b(z)} \tag{3}$$

to maintain charge and current neutrality. This is accompanied by a diamagnetic current at the front and a field compression (Fig. 1b) such that $B(z)/B_o \approx 1 + n_b(z)/n_o$. From Eq. (1a) the reduction in $u_e(z)$ produces a net force $(e\Delta B(z)/M_o c)u_b$ in the positive x-direction which diverts the plasma ions upwards (Fig. 1a). In a high β flow the electrons and the flux follow the path of the ions. For $\Delta \ll R_o$ a change of the plasma frame speed $u_e(z)$ of the order of $\Delta u_e/u_b \approx \Delta/R_o$ is sufficient to establish a quasi-stationary state in which the background magnetoplasma is diverted to one side of the beam. In the laboratory frame the above interaction corresponds to the beam front diverting the ambient plasma and magnetic field sideways and propagating freely. The beam front suffers an erosion due to the energy required to divert the plasma sideways. The resulting loss is, however, minimal for $\beta_b \gg 1$, allowing for long range beam propagation. An important ingredient of this propagation mode is the highly asymmetric steady state. This is contrary to the one expected by fluid or MHD models. It is dominated by kinetic ion effects. The validity of MHD models can only be expected for scale lengths, Δ, larger than the beam or background ion gyroradius. Furthermore, the MHD equations which neglect ion inertial effects yield only symmetric solutions. A fluid treatment which includes ion inertia will allow asymmetric solutions but will miss the highly nonlinear and essentially kinetic ion beam behavior at the beam front. Notice that in the electrostatic (or nondiamagnetic) case [Schmidt, 1960] where $\Delta B \cong 0$ and $\Delta u_e = 0$ flow diversion does not occur and the beam and ambient plasmas will interpenetrate. Interpenetration can cause

instabilities that destroy the coherence of the propagation mode. Such beam dispersal was observed in the laboratory experiments of Birko and Kirchenko [1978] in which an ion acoustic wave was driven unstable on the surface of a low-energy beam in the $\beta_b < 1$ regime, apparently due to the relative drift between heavy and light ions. Similar dispersal was also noted in 2-D particle simulations of cross field ion beam propagation [Shanahan, 1984]. In this case, the wave excitation was attributed to the Buneman instability. The excited surface wave penetrated throughout the bulk of the plasma, was accompanied by strong electron heating and resulted in dispersal of the beam.

In the next section we describe representative results from a series of computer simulations which elucidate the physical description presented above, and help clarify the resulting scaling laws. Of utmost importance in the study is the time over which the beam propagates ballistically. The definition of ballistic propagation depends on the particular application or measurement resolution. For example, if one is concerned with absence of magnetic effects, ballistic propagation will occur over a time scale τ such that the lateral beam displacement $\Delta x_b \ll R_b$. For applications concerned with delivering the beam energy flux at a detector located on a ballistic path at a distance $z_o = u_b t$, the criterion will be $\Delta x_b/\Delta \ll 1$ at $t = z_o/u_b$ (Δ is the lateral beam width). These issues are discussed in Section 5.

Representative Simulation Results

Since the problem is inhomogeneous, two-dimensional, and requires kinetic ion treatment, analytic progress past minor improvements on the above simple and intuitive picture is not possible. We therefore use numerical simulations. A two-dimensional hybrid simulation code is the appropriate tool. The details of the code applied to the problem can be found in Mankofsky et al. [1987]. Briefly, the ions are treated as discrete particles, using standard particle-in-cell techniques to follow their motion in the electromagnetic (EM) fields. Summing over the particles provides the ion charge and current density. The electrons are treated as a massless fluid, described via the momentum and energy equations. These equations, along with the ion equations of motion, are solved self-consistently on a uniform two-dimensional grid for the ion velocity vectors, the EM fields, and the electron pressure, in the nonradiative limit (i.e., Darwin Hamiltonian).

The equations solved in the simulation are:

$$\frac{1}{c}\frac{\partial}{\partial t}\mathbf{B} = -\nabla \times \mathbf{E}$$

and

$$\nabla \times \mathbf{B} = \frac{4\pi}{c}(\mathbf{J}_e + \mathbf{J}_i)$$

The first equation, Faraday's Law, is used to determine the change in magnetic field by inductive electric fields. In the second equation, Ampère's Law, the displacement current has been neglected implying the condition $\nabla \cdot (\mathbf{J}_e + \mathbf{J}_i) = 0$. This in conjunction with quasineutrality, $n_e \simeq n_i$, permits us to determine the velocity, $\mathbf{u}_e$, of the electron fluid as a function of magnetic field and ion current density. Further neglecting electron inertia, but retaining electron pressure and collisionality the electric field is found from force balance for the electrons using a generalized Ohm's Law,

$$\mathbf{E} = -\frac{\mathbf{u}_e}{c} \times \mathbf{B} - \frac{\nabla P_e}{n_i \mid e \mid} - \frac{m_e}{\mid e \mid}\sum_s \nu_{es}(\mathbf{u}_{es} - \mathbf{u}_{es}) \quad .$$

P_e is the electron pressure determined from an appropriate electron energy equation, and ν_{es} is the effective collision frequency with specie "s". The collision frequency can be based on classical Coulomb interaction or used to account for nonlinear plasma coupling through the use of an anomalous prescription. The electric field contains both an electrostatic as well as an inductive component. This model can account for an extremely large range of physical phenomena. It includes ambipolar expansion, magnetic field convection, and magnetic field diffusion. The model resolves Alfv́en waves, whistlers, and kinetic ion effects, and because it is explicit leads to the limitation $\Delta t V^* < \Delta x$, where Δt is the timestep, Δx the smallest cell size, while V^* is the maximum of the Alfv́en and whistler wave phase velocities or the fastest ion velocity in a problem. The omission of electron inertia does not allow a proper treatment of the electron skin depth so we limit our results to scale lengths much greater than c/ω_{pe}.

The system used in the ion beam simulations has periodic boundary conditions in the direction transverse to the flow (i.e., x-axis). In the flow direction (z-axis) plasma is injected from the right boundary at a rate $n_o u_b$ and permitted to leave on the left at the local flux rate. The magnetic field is allowed to float at these boundaries. We describe below simulation results designed to illustrate quantitatively aspects of the high β propagation model.

In the simulations presented here, the ambient plasma was composed of O^+ with density $n_o = 10^5 \#/\mathrm{cm}^3$ and temperature 0.25 eV, and was embedded in a magnetic field $B_o = 0.3$ Gauss. These are parameters typical of the ionospheric F-region. The beam was composed of protons and was given a Gaussian profile in the x and z directions. Beam velocities $u_b = 10^8$, 2×10^8 and 4×10^8 cm/sec were studied, while the total number of beam particles varied

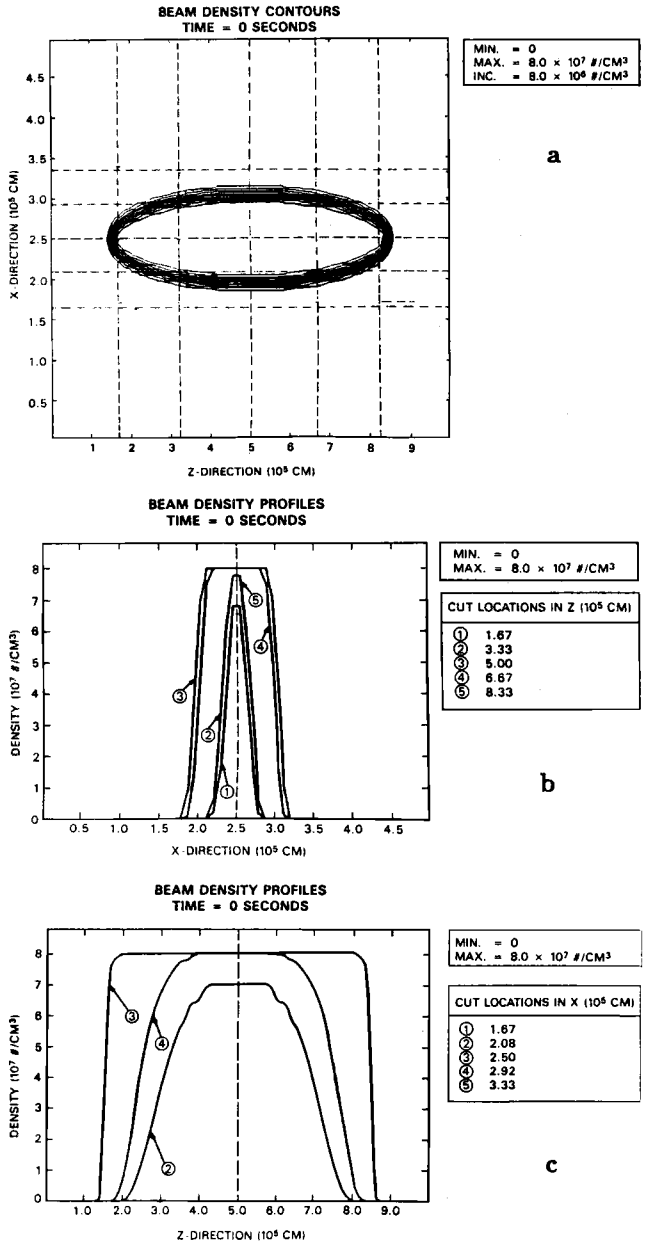

Fig. 2. Initial beam profiles for all runs. The parameters correspond to run #1. For the other runs they can be scaled according to the value of the peak beam density n_b. (a) Beam isodensity contours. This figure shows also the locations of the vertical and horizontal diagnostic cuts in the $x-z$ plane. (b) Beam density profiles along vertical cuts 1-5. (c) Beam density profiles along horizontal cuts 1-5.

between $10^{17} - 10^{19}$, corresponding to peak beam densities in the range of $n_b \approx 5 \times 10^6 - 8 \times 10^7 \#/\text{cm}^3$. Table I lists the parameters of the simulation runs in real (dimensional) and dimensionless units. The runs described here were performed with the magnetic field $\mathbf{B}_o$ out of the plane of the simulation. (Runs were also performed with the magnetic field in the plane of the simulation. We will comment on these later.) All the simulations were performed in the beam reference frame. In this frame, the beam particles are initially stationary while the magnetoplasma flows with $\mathbf{u} = -u_b \hat{e}_z$, with the aid of an appropriate motional electric field. The geometry and the initial conditions of the beam in the simulations are shown in Figs. 2a-c. Figure 2a shows the beam isodensity contours at $t = 0$. To facilitate the understanding of the physics, diagnostic cuts at the positions labeled 1-5 were taken along the x and z axes. Figures 2b, c show the initial beam profiles for cuts 1-5 along the x and z axes. The physics of the interaction described in Section 2 becomes clear by referring to typical simulation results.

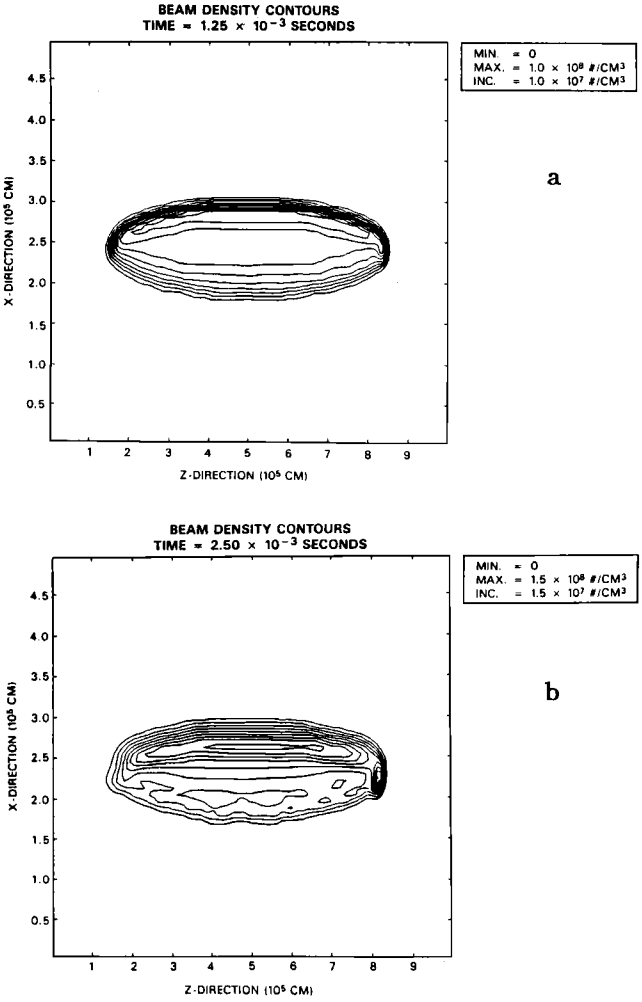

Fig. 3. Isodensity beam contours for run #1. (a) At $t = 1.25$ msec or (equivalently $\Omega_b t = 4$ or propagation distance $4R_b$). (b)At $t = 2.5$ msec.

Run #1 of Table I is examined first. Computer time constraints limited the runs to times $t \leq 2.5$ msec, which corresponds to $\Omega_b t \approx 8$ or propagation distances of 8 R_b ($\Omega_b = eB_o/M_b c = 3 \times 10^3$ sec^{-1} is the proton cyclotron frequency).

The evolution of the beam for the parameters of run #1 can be seen from Figs. 3a, b and 4a, b. Figures 3a, b show the beam isodensity contours at times $t = 1.25$ and 2.5 msec, corresponding to $\Omega_b t = 4$ and 8 and equivalent beam propagation distances of 4 and 8 R_b. It is clear that the beam has maintained its macroscopic integrity as a plasmoid and followed a ballistic trajectory. Similar conclusions are derived from Figs. 4a, b, which show the beam profiles as a function of x at the diagnostic cuts. Figures 4a, b should be compared with Fig. 2b at $t = 0$. Notice that both the isodensity contours and the density profiles show density compression at the center of the beam by almost a factor of two (the vertical scale in the figures changes according to the peak value). Detailed examination of Fig. 4b shows the presence of a secondary density peak at the front of the beam (position #5) which is displaced downwards (i.e. in the negative x-direction). This corresponds to the front erosion discussed in the simplified model of Section 2 and is also apparent at the front in Fig. 3b. The erosion of the beam front provides the momentum that balances the diversion of the flow of the ambient magnetoplasma in the positive x-direction. The erosion rate can be computed quantitatively by resorting to Figs. 2b and 4a, b and examining the temporal evolution of the density of the beam front at diagnostic location 5. The stationary magnetic field structure, which causes the flow diversion, is shown in the form of isomagnetic contours $\Delta\mathbf{B}(x, z)$, i.e. the difference between $\mathbf{B}(x, z)$ and the initial homogeneous $\mathbf{B}_o$, in Figs. 5a, b. Notice the compression of the magnetic field at the front followed by a diamagnetic cavity at the back. As described in Section 2, for $\Delta < R_o$ the

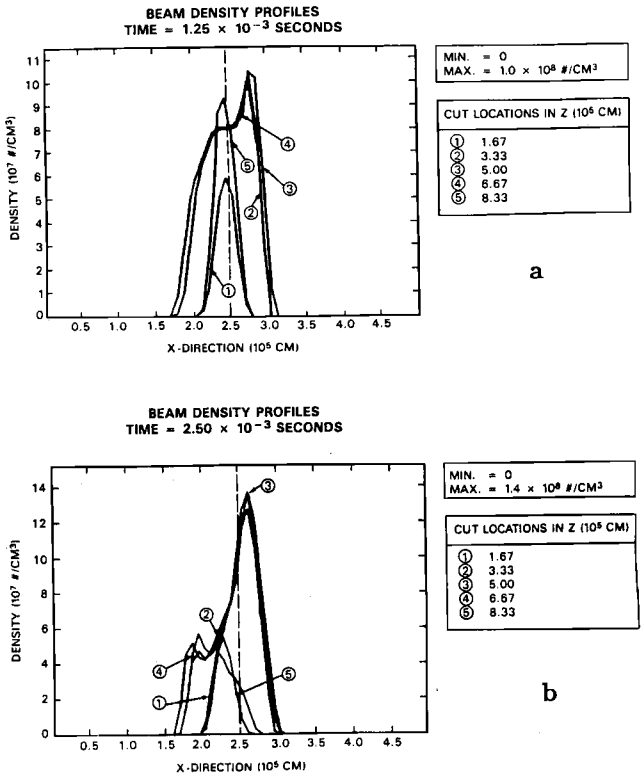

Fig. 4. Vertical beam density profiles at the diagnostic locations for run #1. (a) At $t = 1.25$ msec. (b) At $t = 2.5$ msec.

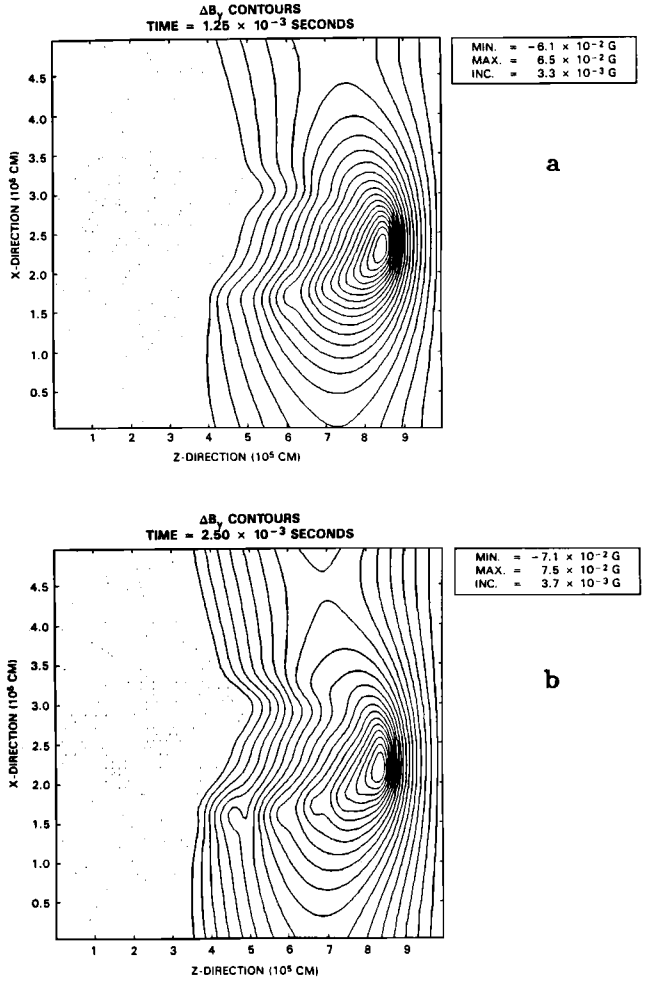

Fig. 5. Isomagnetic contours ΔB for run #1. (Solid lines represent compression of the magnetic field over the ambient, while dotted lines represent magnetic field depression). (a) At $t = 1.25$ msec. (b) At $t = 2.5$ msec.

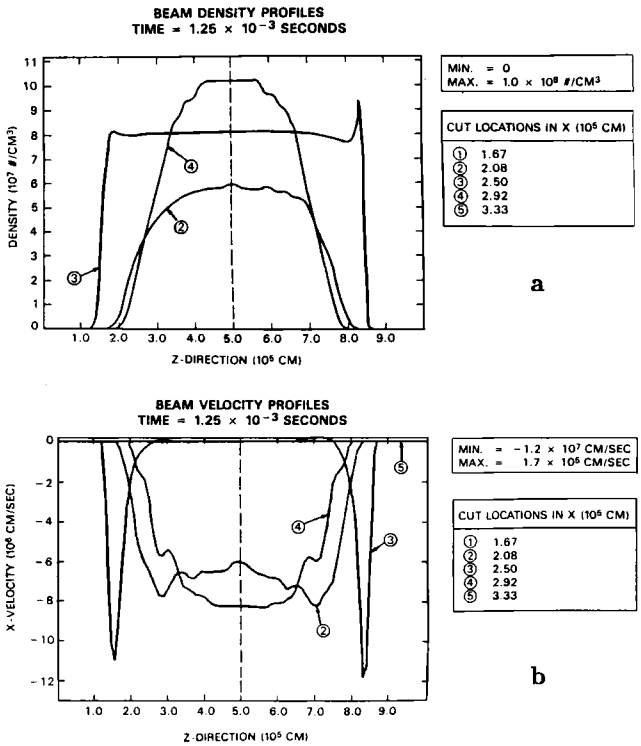

Fig. 6. Horizontal profiles of the beam density (a) and lateral velocity (b) for run #1 at $t = 1.25$ msec.

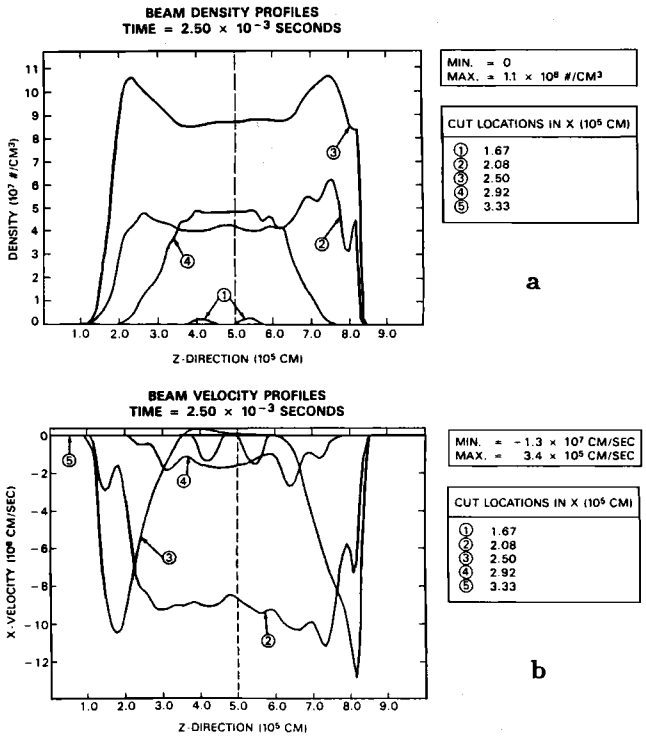

Fig. 7. Same as Fig. 6 at $t = 2.5$ msec.

compression level saturates at the value of $\Delta B/B_o$ necessary to divert the incoming plasma ions sideways to the point that they do not penetrate into the beam. It should be noted that the magnetic field structure, which was set up as early as $\frac{1}{3}\Omega_b^{-1}$, remained essentially stationary over the length of the simulations.

To understand the phenomenology controlling the scaling of the ballistic propagation time scale, we examine the evolution of the horizontal beam density profile (Figs. 6a, 7a) and lateral drift velocity (Figs. 6b, 7b) at the center cut (location #3, representing the maximum of the beam density and momentum flux) at times 1.25 and 2.5 msec. A comparison of Figs. 3a, 6a and 7a in conjunction with Figs. 4a, b shows that the beam density has been compressed at the center point, while the longitudinal length is preserved. Furthermore Figs. 6b and 7b demonstrate that the center of the beam follows a ballistic trajectory (i.e. $u_x = 0$) except at the front and the rear. The front of the beam is eroding at a downward velocity which has saturated at a value $u_x \approx 10^7$ cm/sec. As can be seen by examining the horizontal downward velocity profile at location #3 in Figs. 6b and 7b, the erosion is penetrating backwards towards the beam center.

Let us finally examine the flow behavior of the ambient plasma. Figures 8a, b show the flow speed at $t = 1.25$ and

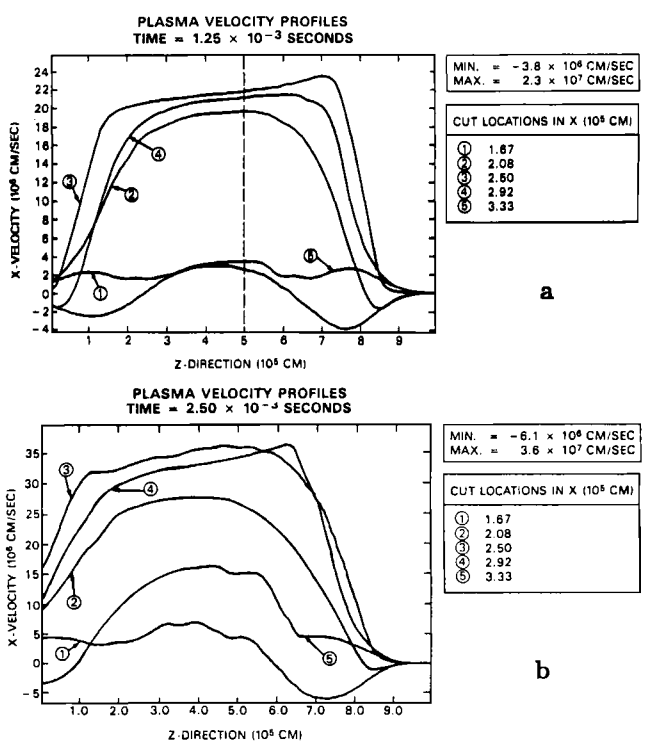

Fig. 8. Horizontal profile of the ambient plasma lateral velocity profiles for run #1. (a) At $t = 1.25$ msec. (b) At $t = 2.5$ msec.

2.5 msec at the horizontal cuts. It can be seen that the plasma is diverted upwards at the front with an increasing speed, reaching a value of about 2×10^7 cm/sec towards the beam center. This implies that if we started with a beam penetrated by ambient plasma, the ambient plasma ions and their neutralizing electrons will move outside the beam. Since, as can be seen in Fig. 8, there is no upward plasma flow from below (i.e. cut #1) toward the beam center, the plasma density inside the beam center will be reduced until there is no more plasma in the beam. This of course will occur only if the front erosion time scale is longer than the plasma evacuation time. We will return to this point later.

Scaling Considerations

The previous discussion identified two critical issues which control the scaling of ballistic beam propagation. The first refers to the scaling of the downward drift of the beam center (i.e. position at the intersection of horizontal and vertical cuts #3) and the upward drift of the plasma. The second refers to the rate of front erosion. As long as the front has not eroded, the beam center will propagate along a trajectory determined by the self-consistent electromagnetic fields at the center of the beam or plasmoid.

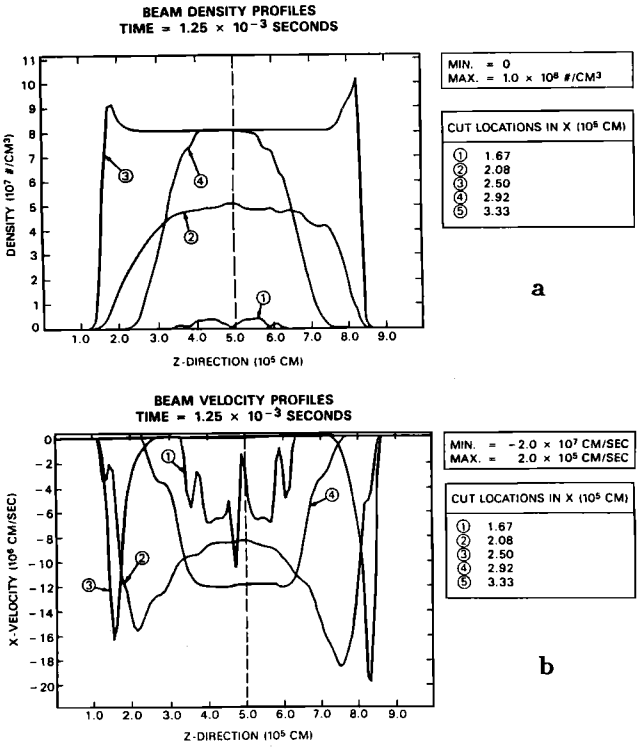

Fig. 9. Horizontal profiles of the beam density (a) and lateral velocity (b) for run #2 at $t = 1.25$ msec.

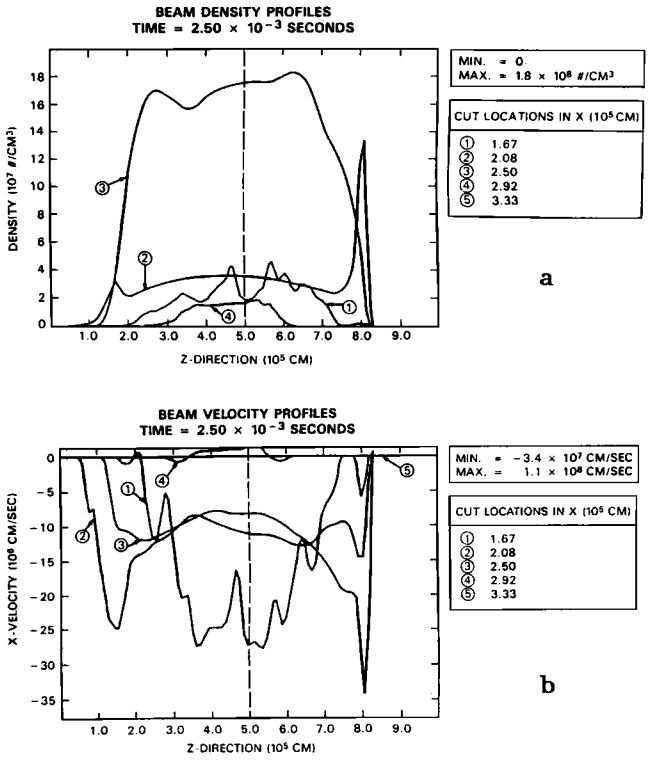

Fig. 10. Same as Fig. 9 at $t = 2.5$ msec.

We examine separately the scaling with beam velocity and with beam density.

Runs #1-3 all have the same number of beam particles (4.8×10^{18}) or an equivalent $n_b/n_o = 800$, but the flow velocity corresponds to 10^8, 2×10^8, and 4×10^8 cm/sec respectively. Figures 9a, b show the horizontal profiles of the beam density and downward displacement at time t=1.25 msec for run #2. The center density profile and center downward velocity are essentially similar to run #1. However, the erosion speed at the front of cut #3 (Fig. 9b) is almost a factor of two faster than in run #1 (i.e. 2×10^7 cm/sec vs 1.1×10^7 cm/sec). This is confirmed by referring to the same profiles at time $t = 2.5$ msec (Figs. 10a, b). While there is still substantial beam density along the center cut #3 (Fig. 10a), the front has eroded to such an extent that the beam center is now drifting downwards at a speed of 10^7 cm/sec. In the above two runs the erosion rate scales almost linearly with u_b. The same trend is evident from an examination of run #3 ($u_b = 4 \times 10^8$ cm/sec). Figure 11 shows the density (a) and downward beam velocity (b) at an earlier time ($t = 0.75$ msec). While the density profile is similar to Figs. 6a and 10a at $t = 1.25$ msec, the downward erosion speed is now 4×10^7 cm/sec, again revealing linear scaling with beam velocity. As a result of the faster erosion rate the profiles at $t = 1.25$ msec (Fig. 12) are

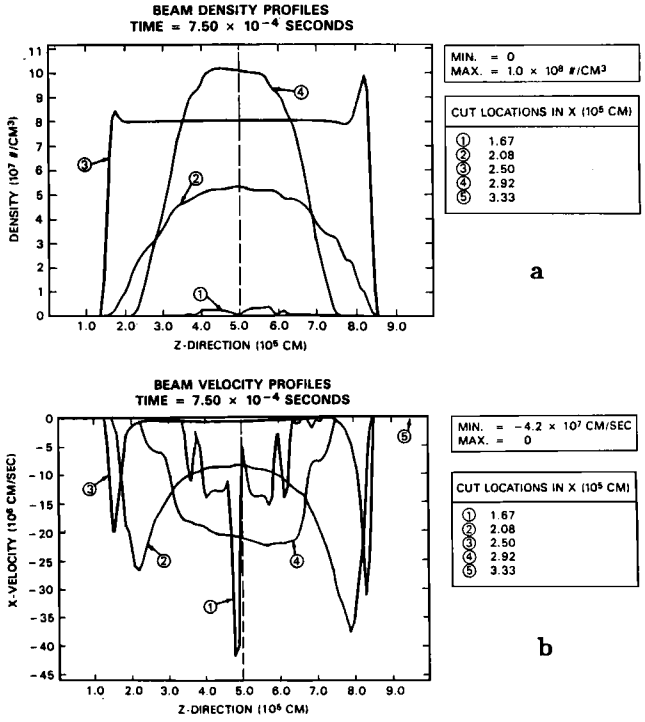

Fig. 11. Same as Fig. 10 for run #1 at $t = 0.75$ msec.

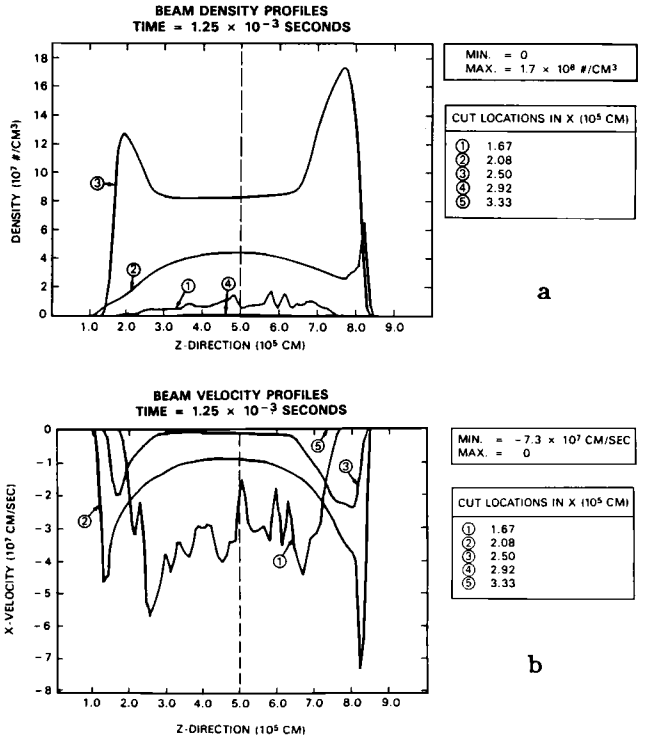

Fig. 12. Same as Fig. 11 at $t = 1.25$ msec.

similar to the ones of run #2 at 2.5 msec (Fig. 11). By time $t = 2.5$ msec the beam has been displaced and modified substantially. However, it has still maintained its plasmoid-like entity, although it is no longer following a ballistic propagation path (Fig. 13a). Figure 13b shows $\Delta\mathbf{B}$ contours at the same time. They should be compared with the contours of the ballistic propagation mode (Fig. 5). Finally, Figs. 14a, b show the plasma flow profiles at $t = 1.25$ msec for runs #2 and #3. It can be seen from these and Fig. 9a that, as expected from the previous results and momentum conservation, the diversion velocity of the plasma at the front as well as the outflow velocity of the plasma from the beam center scale almost linearly with u_b. It should be noted that for the above runs the

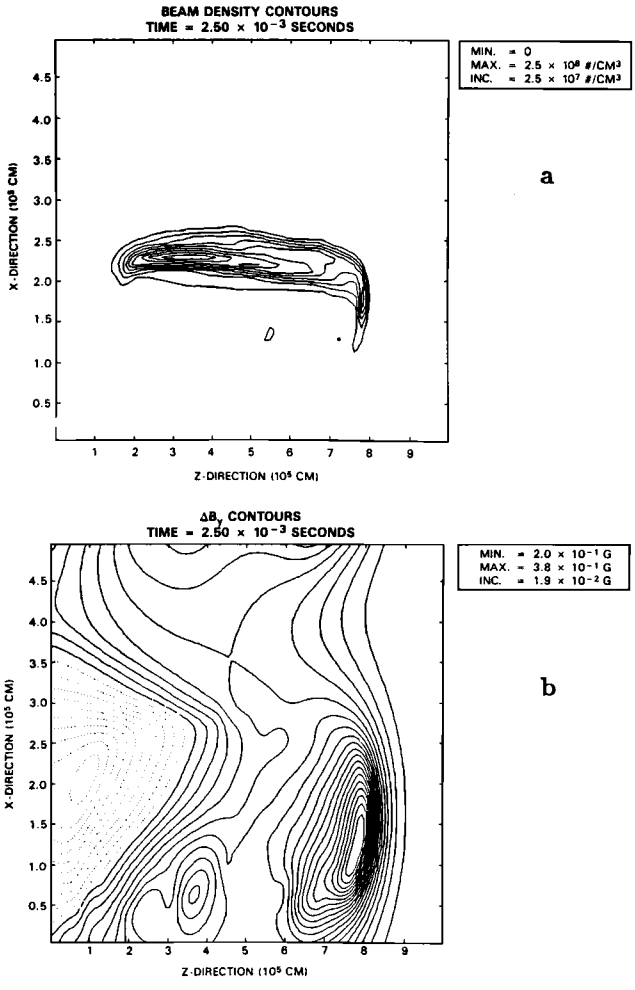

Fig. 13. Isodensity (a) and isomagnetic ΔB (b) contours for run #3 at $t = 2.5$ msec (solid lines represent compression while dashed lines represent depression of the ambient magnetic field).

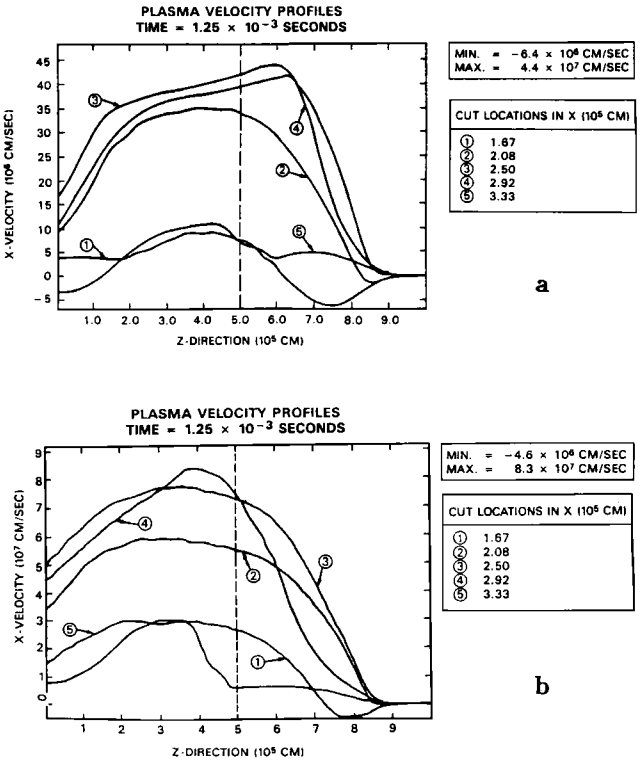

Fig. 14. Horizontal profile of the ambient plasma lateral velocity at $t = 1.25$ msec. (a) For run #2. (b) For run #3.

value of the magnetic field compression at the front also scales linearly with u_b.

We next address scaling issues related to beam-to-plasma density ratios. Runs #1, 4 and 5 all have the same velocity $u_b = 10^8$ cm/sec, but the number of beam particles is 4.8×10^{18}, 1.2×10^{18} and 3×10^{17}, corresponding to $n_b/n_o \approx 800$, 200, and 50. Figures 15a, b and 16a, b show horizontal profiles of beam density and lateral velocity for run #4 at $t = 1.25$ and 2.5 msec. A comparison of Fig. 15 with Fig. 6 shows that over the time scale of $t = 1.25$ msec ($\Omega_b t = 4$) the beam density profiles are basically self-similar for runs #1 and 4. However, in the lower density case (run #4), the center of the beam drifts with $u_x = 2 \times 10^6$ cm/sec while the front erosion speed is 1.7×10^7 cm/sec (Fig 15b). In comparing this with runs #1-3 (Figs. 6b, 9b, 11b) we note that for the high density cases there was essentially no drift of the center of the beam before erosion. The front erosion speeds, however, were $10^7, 2 \times 10^7$ and 4×10^7 cm/sec. Namely, a change in density by a factor of four resulted in a 70% change in the front erosion rate. Referring to Fig. 16 we note that while most of the energy density still remains at the beam center, a combination of a faster erosion rate and a

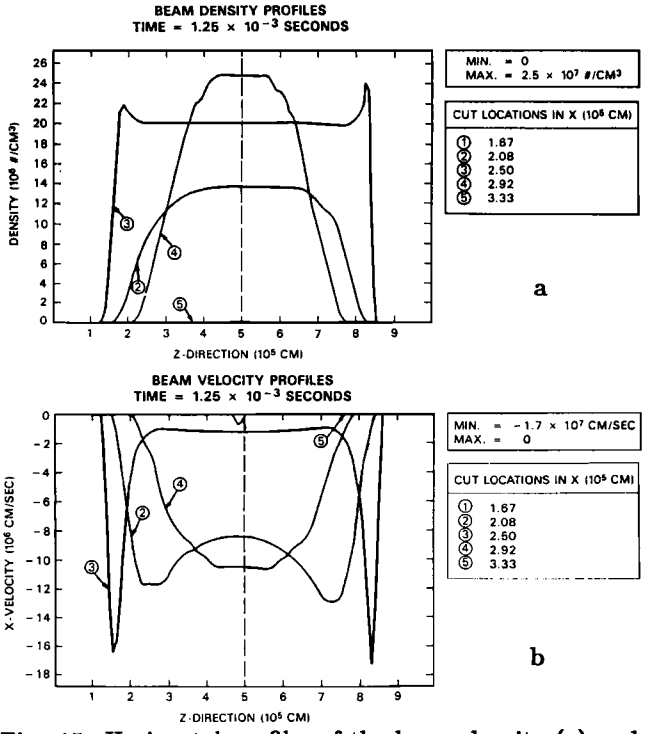

Fig. 15. Horizontal profiles of the beam density (a) and lateral velocity (b) for run #4 at $t = 1.25$ msec.

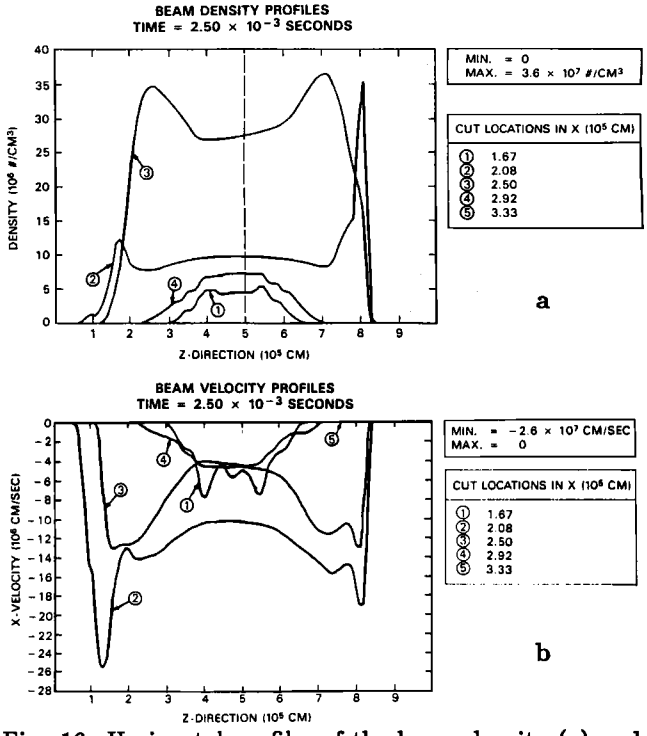

Fig. 16. Horizontal profiles of the beam density (a) and lateral velocity (b) for run #4 at $t = 2.5$ msec.

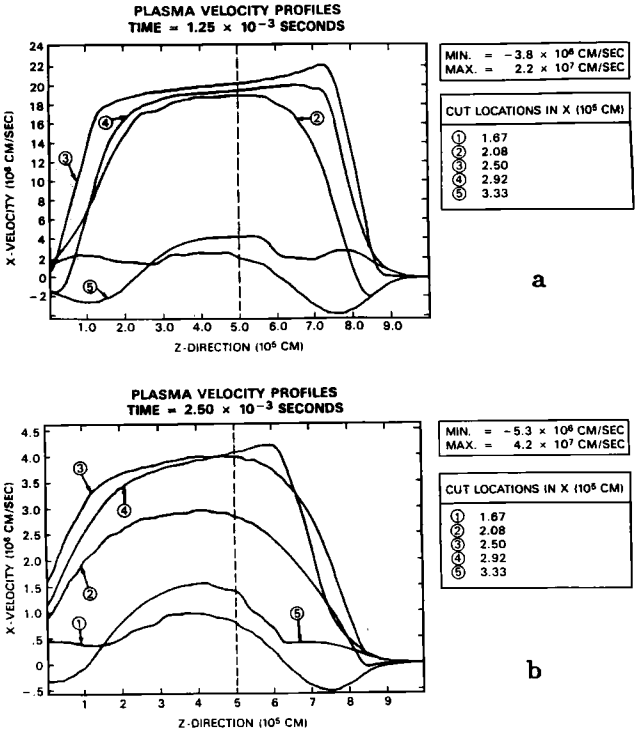

Fig. 17. Horizontal profiles of the ambient plasma lateral velocity for run #4 (a) $t = 1.25$ msec (b) $t = 2.5$ msec.

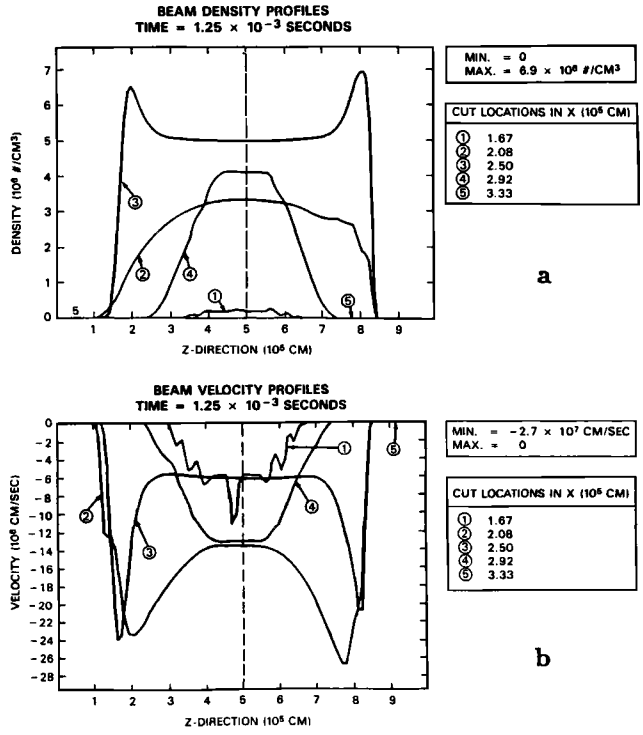

Fig. 18. Horizontal profiles of the beam density (a) and lateral velocity (b) for run #5 at $t = 1.25$ msec.

larger downward displacement of the beam center will destroy the ballistic propagation mode. Figures 17a, b show the velocity displacement profiles of the ambient plasma at $t = 1.25$ and 2.5 msec for run #4. Notice that they are qualitatively and quantitatively similar to the ones for run #1 (Figs. 8a, b). Furthermore, the outflow shows constant acceleration. The above scalings with density continue for the case of run #5 (Figs. 18a, b; 19a, b), which has a factor of four fewer beam particles than run #4 and sixteen times fewer than run #1. It should finally be noted that for the above runs the value of the maximum field compression was approximately the same.

In summary, the simulations described above demonstrate that the presence of a propagating ion beam with $n_b \gg n_o$ sets up an electrodynamic configuration that laterally diverts the ambient plasma in such a fashion that no penetration of the main beam occurs. The lateral diversion speed scales linearly with the beam velocity and is independent of the beam-to-plasma density ratio. Although specific simulation studies with various values of the ambient magnetic field $\mathbf{B}_o$ were not performed, the physical understanding dictates linear scaling of the lateral speed with $\mathbf{B}_o$. The beam responds to this configuration in a manner that is consistent with conservation of momentum in the plasma frame. As a consequence of

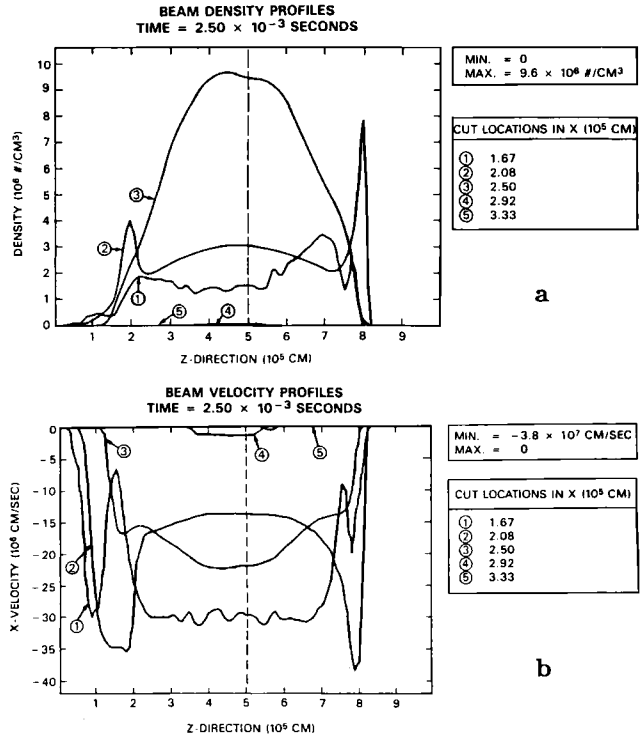

Fig. 19. Horizontal profiles of the beam density (a) and lateral velocity (b) for run #5 at $t = 2.5$ msec.

this, for time scales that are shorter than the front erosion time (i.e. for long thin beams) and for $n_b M_b \gg n_o M_o$, the plasma is evacuated from the central beam region with minimum beam displacement. In fact, the simulations show that the dynamics of the system are such that focusing is produced at the center while momentum is balanced by shedding of surface particles from the beam. The beam will subsequently follow a ballistic path until erosion of the front destroys it. The erosion rate was found to scale linearly with the beam velocity and by the previous argument with $\mathbf{B}_o$, while it is inversely proportional to (n_b/n_o) at the front.

Time Scale for Ballistic Propagation

From the previous analysis we can derive the following general conclusions concerning the time scale for cross field ballistic propagation of a neutralized ion beam of width Δ and length L with density n_b and ion mass M_b.

(i) The plasma will be evacuated from the beam center at an average rate given by

$$\frac{d^2 x_p}{dt^2} = \frac{eE_x}{M_o} \quad , \tag{4}$$

where

$$E_x = u_b \frac{\Delta B}{c} \quad . \tag{5}$$

The evacuation time scale τ_1 for a beam of lateral width Δ is easily computed from Eqs. (4) and (5) as

$$\Omega_b \tau_1 < (2\frac{\Delta}{R_o})^{1/2} \frac{M_o}{M_b} \quad . \tag{6}$$

During this time, the beam displacement Δx_b is given by

$$\frac{\Delta x_b}{\Delta} < \frac{n_b M_b}{n_o M_o} \quad . \tag{7}$$

For times greater than τ_1, no further displacement occurs until the beam front is eroded.

(ii) The front of the beam acts as a shield that allows the bulk of the beam to propagate as described above. The rate of beam erosion can be estimated by simple energy and momentum considerations. The beam erosion rate dz/dt is given by balancing momentum in the z-direction, i.e.

$$n_b M_b \frac{dz}{dt} = n_o M_o (u_b - u_b') \quad , \tag{8}$$

where u_b' is the ambient plasma speed in the z-direction after it has been diverted by the magnetic compression at the front. From conservation of energy,

$$u_b'^2 + u_x^2 = u_b^2 \quad , \tag{9}$$

where u_x is given from Eq. 1a as

$$u_x^2 = 2\frac{e\Delta B}{M_o c} u_b \Delta \tag{10}$$

(i.e. the transverse energy equals the potential drop). For $u_x^2 \ll u_b^2$, i.e. $\Delta/R_o \ll 1$, Eq. (9) becomes

$$u_x^2 = (u_b - u_b')(u_b + u_b') \simeq 2u_b(u_b - u_b') \quad ,$$

so that

$$u_b - u_b' = \Omega_o \frac{\Delta B}{B_o} \Delta \quad . \tag{11}$$

The erosion rate is then found from Eqs. (8) and (11) as

$$\frac{1}{u_b}\frac{dz}{dt} = \frac{n_o M_o}{n_b M_b}\frac{\Delta}{R_o}\frac{\Delta B}{B} < \frac{n_o M_o}{n_b M_b}\frac{\Delta}{R_o} \quad . \tag{12}$$

Notice that for $\Delta/R_o \ll 1$ and $n_o M_o \ll n_b M_b$ the erosion rate is a very small fraction of the beam speed. For a beam of length L we can define a beam erosion time as the time to penetrate to $z = L/2$ from the front. Then Eq. (12) gives an erosion time scale τ_2 as

$$\Omega_b \tau_2 > \frac{1}{2}\frac{n_b}{n_o}\frac{L}{\Delta} \quad . \tag{13}$$

An alternative interpretation of Eq. (12) applies to the case of constant beam injection. Under conditions such that $\Delta z_b/\Delta \ll 1$ as given by Eq. (8), Eq. (12) states that a beam injected into a magnetoplasma with an injection rate faster than the erosion rate will propagate ballistically at all times.

Summary and Conclusions

We presented above a physical model, supported by computer simulation studies, which demonstrated that dense $(n_b M_b \gg n_o M_o)$, thin $(\Delta/R_o \ll 1, \Delta/L \ll 1)$ neutralized ion beams or plasmoids can propagate ballistically if injected in the ionosphere or magnetosphere across the ambient magnetic field. The results presented were based on two-dimensional hybrid simulations performed in the plane perpendicular to the magnetic field. We are in the process of performing three-dimensional simulations as well as extending the simulations of the scaling discussed above to other M_b/M_o ratios, different values of

$\mathbf{B}_o$ and other values of Δ/R_o. These, along with specific applications to active experiments, plasmoid propagation and astrophysical jets, will be published elsewhere.

Before closing we should remark that two-dimensional simulations were also performed with the magnetic field in the simulation plane. Lateral diversion consistent with the earlier simulation results was observed. The only additional feature was that the field lines were slightly draped around the beam as they drifted upwards. As expected, the mode of beam propagation was not affected to any observable degree.

Acknowledgements. The authors are grateful to Drs. R. Sudan, T. Antonsen, P. Wheeler, and J. Denavit for many critical comments and suggestions during the course of this research. This work was supported by the U.S. Department of Energy under contract number DE-AC03-85SF15935.

References

Baker, D.A. and J.E. Hammel, Experimental Studies of the Penetration of a Plasma Stream into a Transverse Magnetic Field, *Phys. Fluids 8*, 713-722 (1965).

Birko, V.F. and G.S. Kirchenko, *Sov. Phys. Tech. Phys. 23*, 202 (1978).

Cargill, P., S. Sarma and K. Papadopoulos, Lower Hybrid Waves and Their Consequences for Cometary Bowshocks, *J. Geophys. Res.* (communicated), 1988.

Chapman, S., Idealized Problems of Plasma Dynamics Relating to Geomagnetic Storms, *Rev. Mod. Phys. 32*, 919-933 (1960).

Chapman, S. and V.C.A. Ferraro, A New Theory of Magnetic Storms, *Terrestrial Magnetism and Atmospheric Electricity 37*, 147-156 (1931).

Ferraro, V.C.A., On the Theory of the First Phase of a Geomagnetic Storm: A New Illustrative Calculation Based on an Idealized (Plane not Cylindrical) Model Field Distribution, *J. Geophys. Res. 57*, 15-49 (1952).

Mankofsky, A., R.N. Sudan, and J. Denavit, *J. Comp. Phys. 70*, 89 (1987).

Papadopoulos, K., A. Mankofsky and A. Drobot, *Phys. Rev. Lett. 61*, 94 (1988).

Peter, W. and N. Rostoker, *Phys. Fluids 25*, 730 (1982).

Schmidt, G., Plasma Motion Across Magnetic Fields, *Phys. Fluids 3*, 961-965 (1960).

Scholer M., On the Motion of Artificial Ion Clouds in the Magnetosphere, *Planet. Space Sc. 18*, 977, 1984.

Shanahan, W. (unpublished), 1984.

Tuck, J.L., Plasma Jet Piercing of Magnetic Fields and Entropy Trapping in a Conservative System, *Phys. Rev. Lett. 3*, 313-315 (1959).